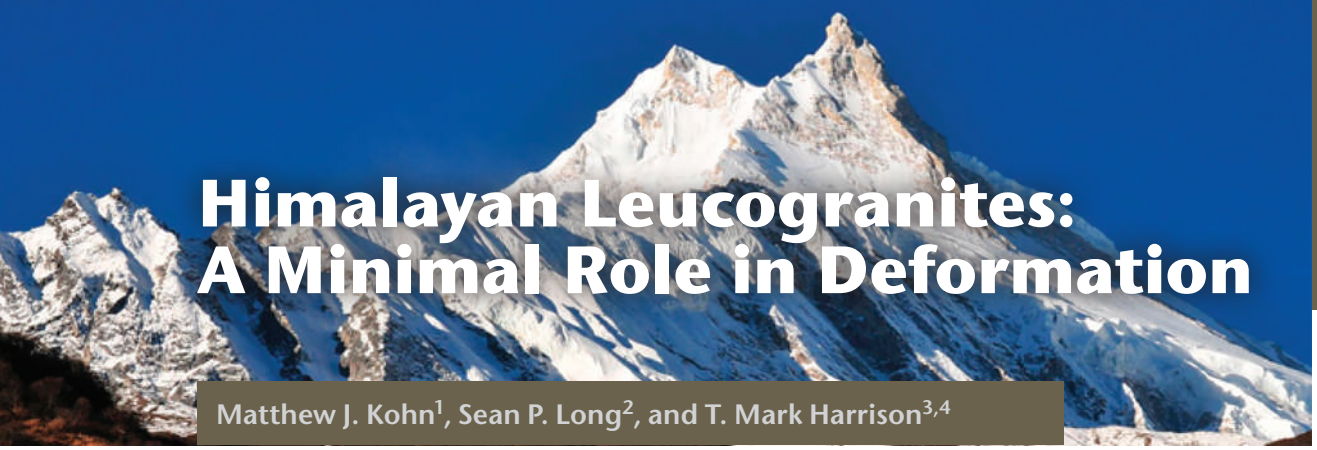

Himalayan Leucogranites: A Minimal Role in Deformation

Mt. Manaslu.
Photo: Patrick Le Fort.

Matthew J. Kohn[1], Sean P. Long[2], and T. Mark Harrison[3,4]

1811-5209/24/0020-0381$2.50 DOI: 10.2138/gselements.20.6.381

A popular model of Himalayan metamorphic and structural evolution argues that partial melting of deeply buried rocks triggered crustal weakening, ductile flow, orogenic collapse, and genesis of leucogranites. Here, we review the origins and evolution of partial melts and leucogranites to demonstrate that they are largely incidental to deformation. Although a pulse of orogenic collapse and leucogranite crystallization occurred at 15–25 Ma, pervasive partial melts formed as much as 20 My earlier. Thus, leucogranites date extraction and transport, not necessarily melting onset. Extensional structures and distributed extensional strain occur in many rocks that lack partial melt and leucogranites, indicating these are not prerequisite to facilitate orogenic collapse. Most mass transfer appears to occur via thrusting, even in partially molten rocks.

Keywords: Greater Himalayan Sequence; partial melt; geothermometry; channel flow; critical taper

INTRODUCTION

Much has been written on the relationships among leucogranites, deformation, and metamorphism in the Himalayan orogen. Key to this discussion is the linking of leucogranites to partial melts (migmatites, which are composite rocks formed by partial melting and found in high-grade metamorphic environments) in the Greater Himalayan Sequence (GHS), which forms the high-grade metamorphic core of the Himalaya (Fig. 1). Isotopic and trace element compositions show that most Himalayan leucogranites were derived from partial melting of the GHS via dehydration-melting reactions (e.g., Harris et al. 1993). This genetic link to the GHS leads to several commonly posed questions (e.g., Searle et al. 2010; Weinberg et al. 2016), including whether exhumation of the GHS triggered melting or melting of the GHS triggered exhumation, whether partial melting occurred simultaneously throughout the GHS, whether melting occurred simultaneously with extensional collapse of the orogen, and whether weakening of a slab of GHS rocks led to large-magnitude, southward 'channel flow' (a tongue of melt-weakened crust, bounded by lower thrust-sense and upper normal-sense ductile shear zones, and flowing between stronger lower and upper crust). Resolving these questions requires investigating the pressure–temperature (P–T) and temperature–time (T–t) histories of the GHS and associated leucogranites, as well as the physical deformation behavior of weakened metamorphic rocks. In this contribution, we review the key characteristics of the Himalaya relevant to this discussion, the distributions of P–T conditions and the T–t evolution of GHS rocks, and the emplacement temperatures and ages of leucogranites, before evaluating how leucogranites and deformation may be linked.

GEOLOGIC OVERVIEW

The Himalaya can be split into three main geologic units (Fig. 1)—the structurally low Lesser Himalayan Sequence (LHS), the intermediate GHS, and the high Tethyan Himalayan Sequence (THS). The LHS and THS are typically greenschist facies or lower, with metamorphic grade increasing rapidly towards the GHS, which reached uppermost amphibolite facies and, rarely, granulite facies (see Yin 2006; Kohn 2014). Major early- to middle-Miocene structures control the first-order distribution of metamorphism and include the Main Central thrust (MCT) and the South Tibetan detachment system (STDS; Fig. 1). The MCT is a ~1–2 km-thick ductile shear zone with >100 km displacement that emplaced high-grade, often partially molten GHS rocks southward over lower-grade LHS rocks. The STDS is a ductile to brittle fault system up to ~2 km thick, which juxtaposed low-grade THS rocks northward onto higher-grade GHS rocks (Fig. 1). Thrust faults that internally deform the GHS package have been proposed on the basis of geochronology, strain gradients, and/or metamorphic P–T conditions (see Larson et al. 2015). To the south, beneath the MCT, Himalayan deformation since the late Miocene has been dominated by construction of the south-directed LHS fold-thrust belt (e.g., Long and Robinson 2021).

One unusual feature of the Himalaya is the presence of two subparallel, syncollisional granite belts, the High Himalayan leucogranites (HHL), which are exposed along the crest of the range, and the North Himalayan granites (NHG), which outcrop ~100 km to the north (Fig. 1). The HHL form a discontinuous chain of generally sill-like bodies beneath the STDS that were emplaced at

1 Boise State University
Department of Geosciences
Boise, ID 83725, USA
E-mail: mattkohn@boisestate.edu

2 Washington State University
School of the Environment
Pullman, WA 99164, USA
E-mail: sean.p.long@wsu.edu

3 University of California, Los Angeles
Department of Earth, Planetary, and Space Sciences
Los Angeles, CA 90095, USA
E-mail: tmh@epss.ucla.edu

4 Institute of Tibetan Plateau Research
Chinese Academy of Sciences
Beijing, 100101, China

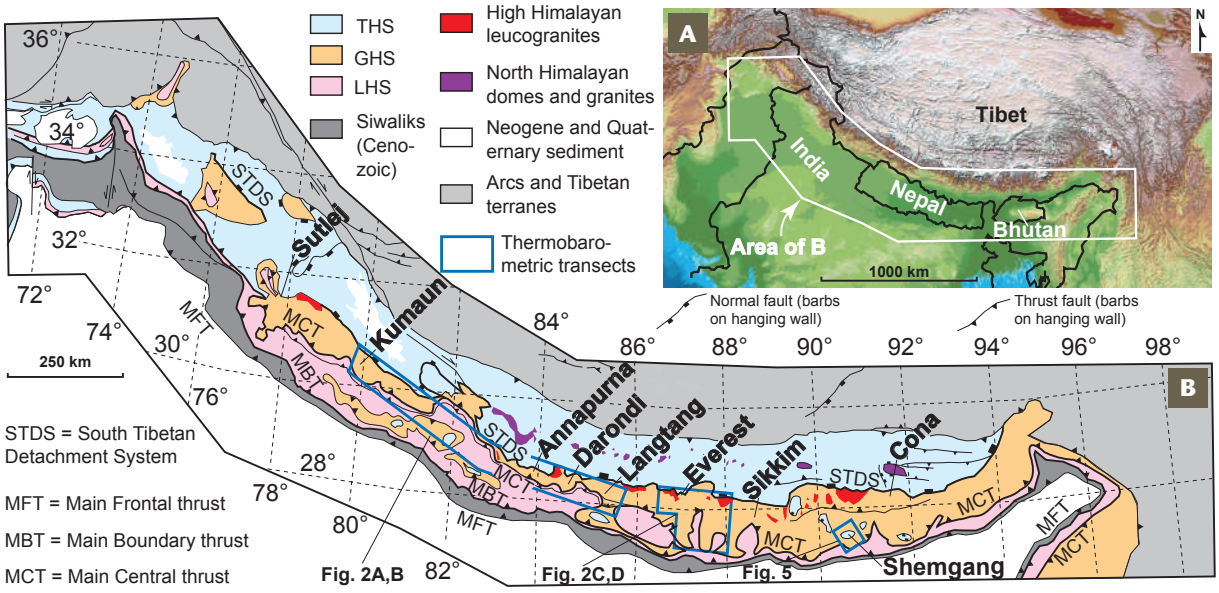

Figure 1 (**A**) Digital elevation model of the Himalaya and neighboring regions. (**B**) Simplified geologic map of the Himalayan orogen, showing main rock units, thermobarometric transects, and key localities discussed in this contribution. Modified after Kohn (2014).

temperatures of ~730 °C or lower (Montel 1993; Harrison et al. 1998; Harrison and Wielicki 2016; see discussion below). Most of the large HHL were emplaced between 23 and 19 Ma (Harrison et al. 1998; Cao et al. 2022). The NHG belt to the north includes leucogranites (Fig. 1) exposed within the cores of structural domes. Reported ages for the NHG range widely (~10 to ~45 Ma; Wu et al. 2020; Cao et al. 2022), but appear to have an age peak between 17 and 19 Ma (Wu et al. 2020), younger than the main phase of HHL emplacement (Harrison et al. 1998). Major NHG plutons also have higher emplacement temperatures than the HHL (Harrison et al. 1998). Like rocks farther south, the STDS in the North Himalayan domes down-drops the THS against the GHS.

The ductile behavior of the GHS and unusual normal-sense shearing along its upper boundary have prompted two principal models for its emplacement between LHS and THS rocks. In channel flow (Beaumont et al. 2001), focused erosion at the orogenic front was coupled with weak middle crust (GHS) to drive southward flow of a ductile channel, with potentially hundreds of kilometers of differential displacement in the channel core relative to rocks above and below. In 'critical taper' (e.g., Robinson and Pearson 2006), the orogen can be described as a wedge in which internal deformation occurs by frictional sliding. In this model, the orogenic wedge grew via southward thrust emplacement, but weakening or changes in boundary conditions induced a north-directed thinning event along the STDS. The occurrence and age of partial melting in the GHS impact these models because partial melting should weaken rocks considerably (e.g., Rosenberg and Handy 2005), which could drive channel flow or wedge collapse. The main question is: relative to motion on the MCT and STDS, what rocks produced partial melts, and when did they produce them? Insofar as leucogranites are linked to partial melting of the GHS, these questions help us understand the genesis of leucogranites and their relationship to deformation.

HOW GHS METAMORPHISM LINKS TO STRUCTURE

One method of identifying major structures and conditions of melting relies on the use of mineral thermobarometry. The most dense thermobarometric datasets can be split into two groups: northwestern India through central Nepal (Fig. 2A, 2B; Kumaun to Langtang), and the Everest region of eastern Nepal (Fig. 2C, 2D). These data from reviews of Kohn (2014) and Goscombe et al. (2018) illustrate the most important thermobarometric trends. Moving structurally upward, temperatures are consistently 500–550 °C in the LHS within 5 km of the GHS, then rise rapidly (within a few km) across the MCT and associated faults to temperatures >750 °C, which, for metashales and metasiltstones, is above the dry solidus (the minimum temperature at which a rock starts to melt in the absence of free water; in this case, the dry solidus corresponds with the muscovite dehydration-melting reaction). Temperatures then gradually increase or remain nearly constant structurally upward, before decreasing at or near the STDS. Overall, thermobarometry confirms that much of the GHS reached *P*–*T* conditions above the dry solidus, and that partial melts must primarily represent dehydration-melting of muscovite, as inferred both geochemically and texturally (e.g., Harris et al. 1993; Kohn 2014). Pressures are more scattered, but generally show nearly constant values in the LHS, increasing dramatically across the MCT and associated faults, then either leveling off or decreasing structurally upward, depending on the specific transect.

How do *P*–*T* conditions relate to deformation? Any generalizations must be tempered with the recognition that each rock undergoes a *P*–*T* evolution, and that the maximum pressure is not always retrieved using standard thermobarometric methods. However, very generally, segments with nearly constant *P* and *T* versus distance are the expected consequence of repeated emplacement of thin thrust sheets, as exemplified within the LHS fold-thrust belt, where thrust-bound packages are evident from distinctive lithologic repetitions, but potentially also for the GHS (e.g., Kohn 2014; Larson et al. 2015), where lithologies are not so distinctive. Segments where pressure decreases more

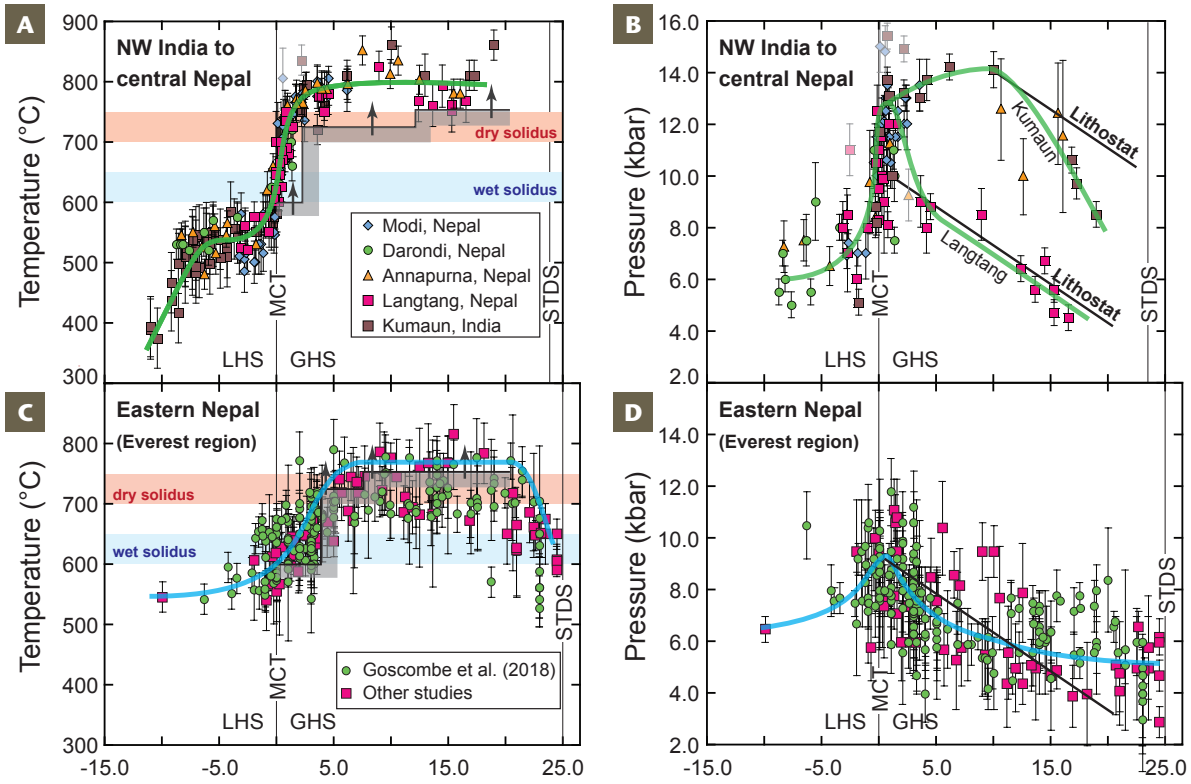

Figure 2 Temperature and pressure versus structural distance from the Main Central thrust (MCT) for NW India to central Nepal (**A**, **B**), and the Everest region of eastern Nepal (**C**, **D**). Data from Kohn (2014), Walters and Kohn (2017), and Goscombe et al. (2018). Gray shaded areas represent phase equilibrium constraints on the stability of staurolite (~575 °C), muscovite dehydration-melting (~700 °C), and cordierite (~725 °C). The scatter in **C** and **D** partly reflects uncertainties in estimating structural distances, which are not reported for data from Goscombe et al. (2018), but also in the method used to calculate *P* and *T*, which has large uncertainties and underestimates temperatures indicated by phase equilibria. GHS = Greater Himalayan Sequence; LHS = Lesser Himalayan Sequence; STDS = South Tibetan Detachment System.

rapidly upward than a lithostatic gradient potentially indicate regions of distributed ductile thinning (e.g., Corrie et al. 2012), such that the measured pressure difference represents a greater thickness of crust than now observed. Finally, regions with rapid changes in *P* and *T* over short distances (e.g., close to the MCT) are expected for structures with large magnitude, long-duration displacement.

TEMPERATURE–TIME HISTORIES OF GHS ROCKS

Another approach for investigating deformation, metamorphism, and their relationship to partial melting relies on trace element systematics in dateable accessory minerals like monazite and zircon. Garnet is a major host for Y and heavy rare-earth elements (HREE: Tb through Lu), so as garnet grows, the Y and HREE concentrations of any newly grown monazite and zircon must generally decrease. Thus, if we plot Y or the sum of HREE (ΣHREE) in monazite or zircon versus time, we expect to see a decrease with time as garnet grows. Because garnets usually grow with increasing *P* and *T* (Fig. 3A), a minimum in Y or HREE in accessory phases should reflect the point of maximum garnet abundance. For many GHS rocks, garnet continues to grow during partial melting as a result of biotite dehydration melting (Fig. 3A), and the point of maximum garnet abundance corresponds to *P*–*T* conditions that are well above the dry solidus (Fig. 3B). Thus, the time of maximum garnet abundance also represents a condition when significant volumes of melt had formed (Fig. 3B). During exhumation and cooling, many garnets are resorbed during retrograde reactions, so we would expect to see Y or HREE in accessory phases increase with time. Finally, because monazite and zircon are somewhat soluble in melts, their latest growth is often interpreted to reflect melt crystallization. In combination, geochronology and trace element geochemistry permit determination of the timing of maximum *P*–*T* conditions and cooling below the solidus.

Dense datasets for accessory mineral geochemistry and geochronology reveal minima in either Y or ΣHREE, and four representative examples are shown in Fig. 3C–3G from the eastern and central Himalaya at different structural levels. These data demonstrate that, in some regions, partial melting must have occurred by ~40 Ma and that maximum *P*–*T* conditions were generally reached earlier at structurally higher levels (e.g., compare Fig. 3D, 3F, and 3G; see also Kohn 2014). However, some reversals in age also occur (e.g., compare Fig. 3E and 3F). These reversals could represent structural repetitions along thrust-sense shear zones, and similar geochronologic data have been used to infer intra-GHS thrusts (e.g., Larson et al. 2015). Several studies now document production of substantial melt in GHS rocks by ca. 35–40 Ma (Fig. 3H, 3I; e.g., Carosi et al. 2015; Walters and Kohn 2017; Ding et al. 2021), but with melt crystallization in leucosomes (the lightest-colored part of a migmatite) generally decreasing in age structurally downward (see summary in Kohn 2014).

TEMPERATURES AND AGES OF LEUCOGRANITES

Ages and melt thermometry (mineral saturation temperatures and Ti-in-zircon thermometry) help place leucogranites into the context of metamorphism and partial melting. Saturation thermometry relies on the dependence of accessory mineral solubility on the major element chemistry of the melt and its temperature. Very generally, mafic rocks dissolve more zircon and monazite than felsic rocks, and solubility increases with increasing temperature (and

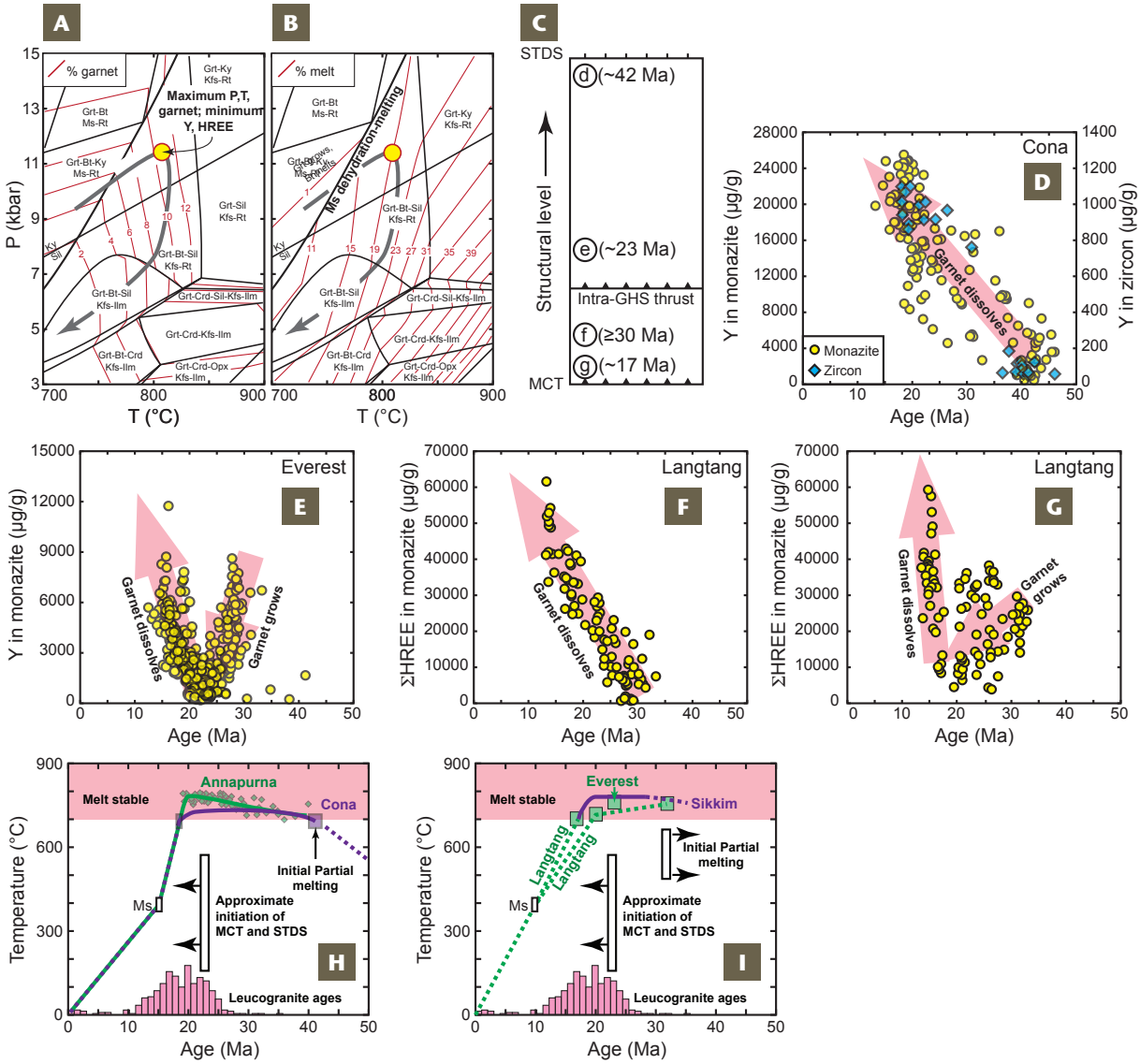

Figure 3 (**A, B**) Typical mineral assemblage diagram for a GHS rock from Groppo et al. (2012), showing mineral stability fields, contoured for abundance of garnet and melt. Maximum *P*–*T* conditions typically represent maximum garnet abundance, above the muscovite-dehydration melting curve. Exhumation should dissolve garnet and possibly increase melt abundance slightly. For most GHS rocks, accessory mineral Y and HREE contents should decrease to a minimum at the maximum *P*–*T* conditions, and increase during exhumation and cooling. (**C**) Schematic section through the GHS, showing positions of samples illustrated in **D**–**G**. (**D**, **E**) Y and (**F**, **G**) ΣHREE content of accessory minerals versus time from four Himalayan localities. Minima generally represent the time at which rocks reached their maximum *P*–*T* condition (prior to exhumation). (**H**, **I**) Temperature–time curves for different areas (dashed where inferred); histogram of leucogranite ages from Cao et al. (2022), excluding North Himalayan domes. Melt-present field is based on typical rock compositions. Geochronologic and geochemical data are from Ding et al. (2021; Cona), Lihter et al. (2023; Everest), Khanal et al. (2020) and Kohn (2014; Langtang), and Kohn (2014) and Walters and Kohn (2017; Annapurna).

water content, for monazite). Once a relationship among temperature, melt composition, and either Zr (Boehnke et al. 2013) or light rare-earth element (LREE: La through Gd; Montel 1993) content is calibrated, a measured whole-rock composition can be used to determine the temperature at which an accessory mineral would have been saturated. However, zircon and monazite in leucogranites commonly retain cores of (undissolved) relict grains. Consequently, whole-rock Zr and LREE contents include not only the fraction that was dissolved in the melt (assumed to be at saturation equilibrium with zircon and monazite), but also extra Zr and LREE from the inherited zircon and monazite. Thus, calculated saturation temperatures may overestimate true magma temperatures.

Summaries of leucogranite chemistry and ages (Wu et al. 2020; Cao et al. 2022) allow monazite and zircon saturation temperatures to be calculated and plotted versus age (Fig. 4A, 4B). Here we distinguish between the High Himalayan leucogranites (e.g., from Cona, Everest, Langtang, etc.; Fig. 4A) and the North Himalayan leucogranites (Fig. 4B). Crystallization in the NHG belt initiated much earlier than the High Himalayan leucogranites and at higher temperatures, especially prior to ~30 Ma. If the North Himalayan leucogranites represent deeper expressions of GHS rocks (because they are farther north in the orogen), they might be expected to have higher temperatures. Monazite saturation temperatures are commonly ~50 °C higher than zircon saturation temperatures (Fig. 4A–4D; Wu et al. 2020).

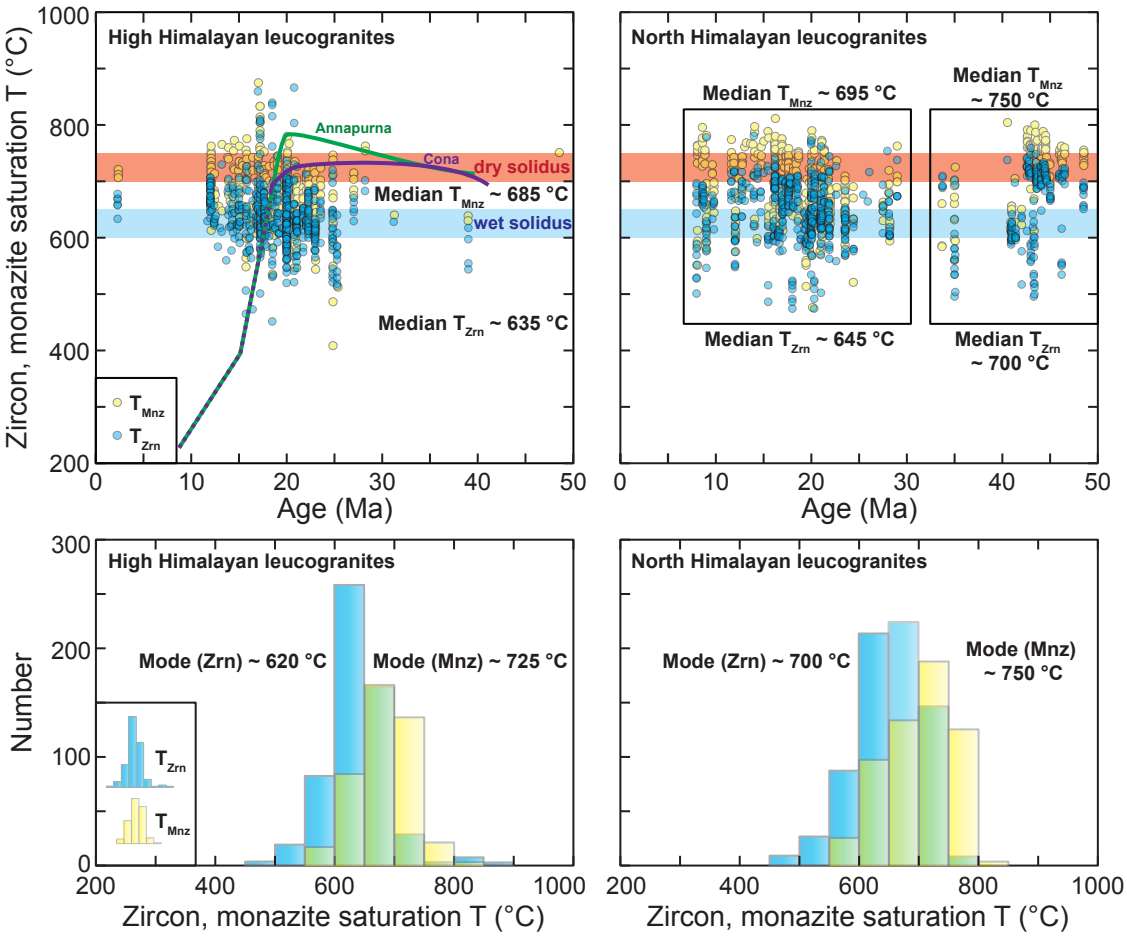

Figure 4 Zircon and monazite saturation temperatures of leucogranites, recalculated from data in Cao et al. (2022) according to methods of Boehnke et al. (2013) and Montel (1993). Calculations assume a typical water content in the melt of 6 wt.% (Montel 1993). Monazite saturation temperatures are generally higher than zircon saturation temperatures, and leucogranites from the North Himalayan domes have higher temperatures than leucogranites from the main belt of GHS rocks. Most temperatures are below the dry solidus, and many are below the wet (i.e., water-saturated) solidus, implying that most leucogranites are not primary melts of the GHS. Temperature–time curves for Annapurna and Cona are shown for reference.

DISCUSSION

How do Himalayan Leucogranites Relate to Metamorphism?

The relationship between Himalayan leucogranites and metamorphism is indirect. First, although isotope and trace element data, plus field relations, clearly demonstrate that leucogranites derive from GHS rocks, they are not likely direct samples of exposed GHS partial melts. Typical partial melts in the GHS formed at temperatures ≥750 °C (Fig. 2), whereas apparent saturation temperatures of leucogranites and trace element thermometry in zircon are typically 100 °C lower (Fig. 4; Kohn 2014). These data imply that most leucogranites either evolved from higher-temperature GHS melts, e.g., through fractional crystallization during cooling (Wu et al. 2020), or they preferentially tapped atypically cool GHS rocks, possibly at lower structural levels (Harrison et al. 1998).

Second, crystallization ages of Himalayan leucogranites may say little about the timing of melting. Prior studies have equated a pulse of leucogranite crystallization starting at ~24 Ma with initiation of GHS melting (e.g., Searle et al. 2010; Weinberg 2016). However, zircon and monazite ages reported for most igneous bodies represent the timing of crystallization of separated melts, not melting. Partial melts can exist for millions or tens of millions of years before they segregate and crystallize. Thus, the pulse of leucogranite ages between 15 and 25 Ma (Figs. 3 and 4) may represent a pulse of melt *extraction, transport, and crystallization*, not necessarily a pulse of melting. Even if the leucogranites do record a 15–25 Ma melting pulse, partial melts had already formed as much as 20 My earlier (e.g., Kohn 2014; Walters and Kohn 2017; Ding et al. 2021; Fig. 3). In principle (e.g., Rosenberg and Handy 2005; Diener and Fagereng 2014), extraction of melts could strengthen the crust, as weak melts are removed from the mid- to lower-crust to crystallize as strong feldspar-rich granites in the upper crust.

How do Himalayan Leucogranites Relate to Deformation?

The closest link between Himalayan leucogranites and deformation lies in the likely synchroneity among motion on the STDS, motion on underlying GHS thrusts, and the pulse of leucogranite extraction and crystallization. There is clear evidence for motion along the STDS and thrusts near the base of the GHS, including the MCT, by 22–24 Ma until perhaps 16–13 Ma (e.g., Yin 2006; Kohn 2014; Kellett et al. 2018). Studies that have inferred older ages for STDS movement have major interpretational ambiguities. For example, a commonly quoted age of STDS initiation of ~35 Ma (Lee and Whitehouse 2007) assumes that the oldest zircon rim ages in a partially melted rock represent final melt crystallization. But zircon ages in partially melted rocks can easily span 20 My (e.g., Fig. 2D) and, in fact, ranged down to ~25 Ma in the analyzed rock. Other rocks in the area are consistent with initial STDS motion at 23 Ma. Movement on thrust faults near the base of the GHS (which was cooler; Fig. 2) could have catalyzed new partial melting

in underthrusted footwall rocks (e.g., Fig. 3E, 3G) to form the HHL at 19–23 Ma and the NHG a few million years later (Harrison et al. 1998). Overall, although there is temporal congruence between fault movement and emplacement of leucogranites, there is little evidence that formation of partial melts catalyzed fault movement.

What Drove Partial Melting?

Many metamorphic studies show maximum *P*–*T* conditions in the GHS above muscovite dehydration-melting at depths of 40–50 km (e.g., Groppo et al. 2012; Rubatto et al. 2013; Kohn 2014; Walters and Kohn 2017; Ding et al. 2021; Figs. 2 and 3), which would generate substantial partial melt (Fig. 3B). Many thermodynamic models show that subsequent exhumation would increase the volume fraction of melt only slightly (Fig. 3B). Consequently, most melting likely occurred because the GHS was buried deeply, albeit with possible important additions from strain heating (Harrison et al. 1998). For example, a typical thermal gradient (the rate of change in temperature with respect to increasing depth in Earth's interior) in the Himalaya was only ~20 °C/km, which is fairly cold. Although the Himalaya are sometimes called a large hot orogen, melting in many areas occurred, not because of an unusually high thermal gradient, but because muscovite-rich rocks were abundant and buried so deeply. Trace element data in monazite, zircon, and titanite further demonstrate that melting in the GHS, especially at higher structural levels, preceded intrusion and crystallization of leucogranites and displacement on the STDS (e.g., Rubatto et al. 2013; Kohn 2014; Carosi et al. 2015; Walters and Kohn 2017; Khanal et al. 2020; Ding et al. 2021). Therefore, although collapse of the orogen and associated decompression may have catalyzed melt extraction and intrusion, it probably did not contribute substantially to melt formation.

How is Deformation Linked to Rock Strength, Partial Melts, and Leucogranites?

Both channel flow and collapse of a critically tapered wedge can be explained if the metamorphic core of an orogen weakens past a strength threshold. Because partial melting decreases rock strength (Rosenberg and Handy 2005), GHS melting could potentially explain orogenic collapse, southward flow, and formation of the STDS. If so, the Himalaya must have accumulated a sufficient volume fraction of melt over a sufficiently large along-strike length to trigger orogenic collapse. Presumably, the orogen would have crossed this threshold soon after ~25 Ma, as this is when initial motion on the STDS is first well-documented (e.g., Kellett et al. 2018). In detail, it is hard to reconcile channel flow models *sensu stricto* (Beaumont et al. 2001) with metamorphic and geochronologic observations (e.g., Harrison 2006; Kohn 2014). We will not repeat those arguments in detail here, but they boil down to inconsistencies between the *P*–*T*–*t* predictions of channel flow in comparison with observations, and a lack of evidence that GHS rocks were underthrusted beneath Tibet before they partially melted. Instead, here we emphasize that, in several places in the orogen, distributed strain patterns and the deformation style recorded in the GHS and THS are also difficult to reconcile with channel flow models, and the STDS is locally spatially decoupled from partial melting and leucogranites.

Regarding the deformation style of the GHS, in several places across the orogen (most notably Nepal), the GHS was assembled by progressive imbrication of ductile thrust sheets, with intra-GHS, thrust-sense shear zones defined by metamorphic, strain, and/or geochronologic discontinuities (e.g., Larson et al. 2015). This deformation style is consistent with critical taper models. Intra-GHS thrust imbrication locally initiated as early as ~30 Ma, prior to motion on the STDS, and locally continued until as late as ~10 Ma, outlasting leucogranite and melt crystallization and STDS motion (Larson et al. 2015).

Regarding strain patterns, in the Shemgang region of central Bhutan, strain data demonstrate that distributed, north-directed, extensional shearing above the MCT was accommodated in both GHS and THS rocks, and achieved substantial ductile thinning (Long et al. 2017; Fig. 5). Evidence is lacking for partial melts in the THS and in much of the GHS, suggesting that strain was not strongly partitioned into partially molten rocks. Thermobarometry confirms strain measurements and shows that this 10-km-thick section was originally nearly 20 km thick (Corrie et al. 2012). Notably, thinning was not restricted to partial melt-bearing GHS rocks, but also affected a thick overlying package of GHS rocks that lack melt and leucogranites, as well as lower-grade THS rocks. Thus, at least in central

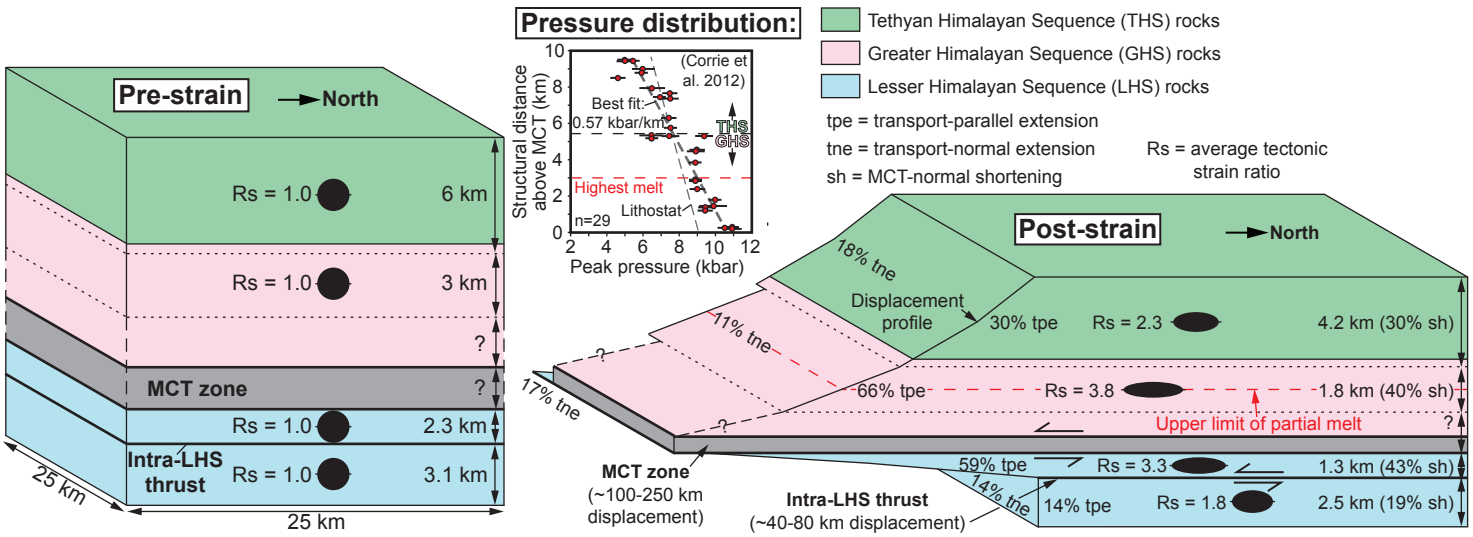

Figure 5 Block diagrams illustrating distributed strain and pressure patterns through the GHS and THS in central Bhutan. Although hot rocks with partial melts generally exhibit larger strain magnitudes, substantial strain was taken up in overlying rocks that lack partial melts and leucogranites. These observations suggest that penetrative strain is not strongly partitioned into partially molten rocks. Modified from Long et al. (2017).

Bhutan, pervasive ductile thinning (orogenic collapse) does not appear directly linked to partial melting and leucogranite emplacement.

Additionally, several isolated exposures of the STDS have been mapped in Nepal and Bhutan that are located as much as ~100–150 km south of the primary northern trace of the STDS (Fig. 1) (e.g., Kellett et al. 2018). These isolated exposures of the STDS typically overlie much thinner GHS packages, some of which lack evidence for partial melt in proximity to the STDS trace, and most of which lack large leucogranite bodies. This further diminishes the importance of leucogranites and partial melt as necessary prerequisites linked to orogenic collapse via motion on the STDS.

OUTSTANDING QUESTIONS

The recent combination of trace element geochemistry with geochronology and metamorphic petrology has revealed numerous details about the assembly of the Himalaya. Nonetheless, major questions still remain. Complete detailed *P*–*T* and structural transects across the GHS are lacking in many places, so we do not know the degree to which the GHS represents multiple thrust sheets with distinct *P*–*T*–*t* histories (more consistent with critical taper) or if it behaved more systematically from bottom to top (more consistent with channel flow). We also do not know the timing of melt initiation outside of a few localities, even though this is critical for evaluation of dynamic models of orogenesis. The initial timing of motion on the STDS is also surprisingly difficult to constrain. Finally, comparisons of strain distributions through the GHS and their consistency (or lack thereof) with metamorphism and the predictions of channel flow models are sparse and deserve further scrutiny.

ACKNOWLEDGMENTS

We thank Victor Guevara and Chris Spencer for their incisive reviews, as well as Fu-Yuan Wu and Fangzhen Teng for inviting this contribution, and Janne Blichert-Toft for careful editing. Funded through NSF grants EAR 2118114 (to MJK) and EAR 2118117 (to SPL), and NSF EAR's Instrumentation and Facilities Program (to TMH).

REFERENCES

Beaumont C, Jamieson RA, Nguyen MH, Lee B (2001) Himalayan tectonics explained by extrusion of a low-viscosity crustal channel coupled to focused surface denudation. Nature 414: 738-742, doi: 10.1038/414738a

Boehnke P, Watson EB, Trail D, Harrison TM, Schmitt AK (2013) Zircon saturation re-revisited. Chemical Geology 351: 324-334, doi: 10.1016/j.chemgeo.2013.05.028

Cao HW and 11 coauthors (2022) Himalayan leucogranites: a review of geochemical and isotopic characteristics, timing of formation, genesis, and rare metal mineralization. Earth-Science Reviews 234: 104229, doi: 10.1016/j.earscirev.2022.104229

Carosi R and 9 coauthors (2015) Eocene partial melting recorded in peritectic garnets from kyanite-gneiss, Greater Himalayan Sequence, central Nepal. Geological Society, London, Special Publications 412: 111-129, doi: 10.1144/sp412.1

Corrie SL, Kohn MJ, McQuarrie N, Long SP (2012) Flattening the Bhutan Himalaya. Earth and Planetary Science Letters 349-350: 67-74, doi: 10.1016/j.epsl.2012.07.001

Diener JFA, Fagereng Å (2014) The influence of melting and melt drainage on crustal rheology during orogenesis. Journal of Geophysical Research: Solid Earth 119: 6193-6210, doi: 10.1002/2014JB011088

Ding H, Kohn MJ, Zhang Z (2021) Long-lived (ca. 22–24 Myr) partial melts in the eastern Himalaya: petrochronologic constraints and tectonic implications. Earth and Planetary Science Letters 558: 116764, doi: 10.1016/j.epsl.2021.116764

Goscombe B, Gray D, Foster DA (2018) Metamorphic response to collision in the Central Himalayan orogen. Gondwana Research 57: 191-265, doi: 10.1016/j.gr.2018.02.002

Groppo C, Rolfo F, Indares A (2012) Partial melting in the Higher Himalayan crystallines of eastern Nepal: the effect of decompression and implications for the 'channel flow' model. Journal of Petrology 53: 1057-1088, doi: 10.1093/petrology/egs009

Harris N, Massey J, Inger S (1993) The role of fluids in the formation of High Himalayan leucogranites. In: Treloar PJ, Searle MP (eds) Himalayan Tectonics. Geological Society, London, Special Publication, London, pp 391-400, doi: 10.1144/GSL.SP.1993.074.01.26

Harrison TM, Grove M, Lovera OM, and Catlos EJ (1998) A model for the origin of Himalayan anatexis and inverted metamorphism. Journal of Geophysical Research 103: 27017-27032, doi: 10.1029/98JB02468

Harrison TM (2006) Did the Himalayan crystallines extrude partially molten from beneath the Tibetan plateau? In: Law RD, Searle MP, Godin L (eds) Channel Flow, Ductile Extrusion and Exhumation in Continental Collision Zones. Geological Society, London, Special Publications 268, London, pp 237-254, doi: 10.1144/GSL.SP.2006.268.01.11

Harrison TM, Wielicki MM (2016) From the Hadean to the Himalaya: 4.4 Ga of felsic terrestrial magmatism. American Mineralogist 101: 1348-1359, doi: 10.2138/am-2016-5516

Kellett DA, Cottle JM, Larson KP (2018) The South Tibetan Detachment System: history, advances, definition and future directions. Geological Society, London, Special Publications 483: 377-400, doi: 10.1144/sp483.2

Khanal GP, Wang JM, Wu FY, Wang JG, Yang L (2020) In-sequence buoyancy extrusion of the Himalayan Metamorphic Core, central Nepal: constraints from monazite petrochronology and thermobarometry. Journal of Asian Earth Science 199: 104406, doi: 10.1016/j.jseaes.2020.104406

Kohn MJ (2014) Himalayan metamorphism and its tectonic implications. Annual Review of Earth and Planetary Sciences 42: 381-419, doi: 10.1146/annurev-earth-060313-055005

Larson KP, Ambrose TK, Webb AAG, Cottle JM, Shrestha S (2015) Reconciling Himalayan midcrustal discontinuities: the Main Central thrust system. Earth and Planetary Science Letters 429: 139-146, doi: 10.1016/j.epsl.2015.07.070

Lee J, Whitehouse MJ (2007) Onset of mid-crustal extensional flow in southern Tibet: evidence from U/Pb zircon ages. Geology 35: 45-48, doi: 10.1130/g22842a.1

Lihter I, Larson KP, Shrestha S, Cottle JM (2023) Tectonometamorphic evolution of the Himalayan metamorphic core in the Makalu–Arun region, eastern Nepal. Journal of the Geological Society 180: doi: 10.1144/jgs2022-056

Long SP, Gordon SM, Soignard E (2017) Distributed north-vergent shear and flattening through Greater and Tethyan Himalayan rocks: insights from metamorphic and strain data from the Dang Chu region, central Bhutan. Lithosphere 9: 774-795, doi: 10.1130/l655.1

Long SP, Robinson DM (2021) Construction of the Lesser Himalayan–Subhimalayan thrust belt: the primary driver of thickening, exhumation, and high elevations in the Himalayan orogen since the middle Miocene. Geology 49: 1283-1288, doi: 10.1130/g48967.1

Montel JM (1993) A model for monazite/melt equilibrium and application to the generation of granitic magmas. Chemical Geology 110: 127-146, doi: 10.1016/0009-2541(93)90250-M

Robinson DM, Pearson ON (2006) Exhumation of Greater Himalayan rock along the Main Central thrust in Nepal: implications for channel flow. Geological Society, London, Special Publications 268: 255-267, doi: 10.1144/GSL.SP.2006.268.01.12

Rosenberg CL, Handy MR (2005) Experimental deformation of partially melted granite revisited: implications for the continental crust. Journal of Metamorphic Geology 23: 19-28, doi: 10.1111/j.1525-1314.2005.00555.x

Rubatto D, Chakraborty S, Dasgupta S (2013) Timescales of crustal melting in the Higher Himalayan crystallines (Sikkim, Eastern Himalaya) inferred from trace element-constrained monazite and zircon chronology. Contributions to Mineralogy and Petrology 165: 349-372, doi: 10.1007/s00410-012-0812-y

Searle MP, Cottle JM, Streule MJ, Waters DJ (2010) Crustal melt granites and migmatites along the Himalaya: melt source, segregation, transport and granite emplacement mechanisms. Earth and Environmental Science Transactions of the Royal Society of Edinburgh 100: 219-233, doi: 10.1017/s175569100901617x

Walters JB, Kohn MJ (2017) Protracted thrusting followed by late rapid cooling of the Greater Himalayan Sequence, Annapurna Himalaya, Central Nepal: insights from titanite petrochronology. Journal of Metamorphic Geology 35: 897-917, doi: 10.1111/jmg.12260

Weinberg RF (2016) Himalayan leucogranites and migmatites: nature, timing and duration of anatexis. Journal of Metamorphic Geology 34: 821-843, doi: 10.1111/jmg.12204

Wu FY and 10 coauthors (2020) Highly fractionated Himalayan leucogranites and associated rare-metal mineralization. Lithos 352-353: 105319, doi: 10.1016/j.lithos.2019.105319

Yin A (2006) Cenozoic tectonic evolution of the Himalayan orogen as constrained by along-strike variation of structural geometry, exhumation history, and foreland sedimentation. Earth-Science Reviews 76: 1-131, doi: 10.1016/j.earscirev.2005.05.004 ■